PCCP

PAPER

Cite this: *Phys. Chem. Chem. Phys.*, 2018, **20**, 26570

Evaluation of the formation and carbon dioxide capture by Li_4SiO_4 using *in situ* synchrotron powder X-ray diffraction studies†

M. L. Grasso,[a] M. V. Blanco,[b] F. Cova,[b] J. A. González,[c] P. Arneodo Larochette[a] and F. C. Gennari *[a]

Received 8th June 2018,
Accepted 26th September 2018

DOI: 10.1039/c8cp03611j

rsc.li/pccp

Carbon capture and storage using regenerable sorbents are an effective approach to reduce CO_2 emissions from stationary sources. In this work, lithium orthosilicate (Li_4SiO_4) was studied as a carbon dioxide sorbent. For a deeper understanding of the synthesis and carbonation mechanism of Li_4SiO_4, an *in situ* synchrotron radiation powder X-ray diffraction technique was used. The Li_4SiO_4 powders were synthesized by a combination of ball milling of a Li_2CO_3 and SiO_2 mixture followed by a thermal treatment process at low temperature. *In situ* studies showed that formation of Li_4SiO_4 from the as-milled $2Li_2CO_3$–SiO_2 mixture involves decomposition of Li_2CO_3 by reaction with SiO_2 *via* Li_2SiO_3 as an intermediate compound. No evidence of $Li_2Si_2O_5$ formation was obtained, in spite of thermodynamic predictions. The CO_2 capture by Li_4SiO_4 was evaluated dynamically over a wide temperature range, reaching a maximum weight increase of 34 wt% and good cyclability after about 10 cycles. By thermogravimetric and microstructural analyses in combination with *ex situ* and *in situ* measurements, a two step carbonation mechanism and its influence on the final CO_2 capture was clearly elucidated. Under dynamical conditions up to 700 °C, the lower number of Li_2CO_3 nuclei initially formed retards the double shell formation and the nucleation and growth of the Li_2CO_3 particles remains the controlling step up to higher CO_2 capture capacity. Isothermal carbonation at 700 °C favours the formation of a higher number of Li_2CO_3 nuclei that creates a thin carbonate shell. The CO_2 diffusion through this shell is the limiting step from the beginning and further carbonation is hindered as the reaction progresses.

1. Introduction

The growing emission of gases responsible for the greenhouse effect is one of the environmental problems that has attracted the most attention in recent decades. Between 1750 (the Industrial Revolution) and 2011, cumulative anthropogenic CO_2 emissions in the atmosphere were 2040 ± 310 $GtCO_2$.[1] About 40% of these emissions remained in the atmosphere; the rest was stored on the land and in the ocean. CO_2 emissions due to fossil fuel combustion and industrial processes account for about 80% of the total anthropogenic gases associated with the greenhouse effect.[1] Globally, economic and population growths continue to be the most important drivers of increases in CO_2 emissions due to the combustion of fossil fuels (coal, oil, and natural gas). However, while the contribution of the population growth between 2000 and 2010 remained constant with respect to the previous three decades, the contribution of the economic growth has risen sharply. For these reasons, one of the challenges facing the scientific community is to provide possible solutions that contribute to the reduction of CO_2 emissions caused by human activity.

One of the most attractive options to reduce the emissions of CO_2 in the atmosphere is the development of technologies for CO_2 capture and storage at the generation site.[2,3] There are currently three CO_2 capture processes that can be used in coal- and gas-fired power plants: pre-, post- and oxy-combustion.[3,4] In particular, the post-combustion capture of CO_2 using liquid sorbents, such as amine scrubbing, is a mature technology that has been proven effective over the past 50 years. However, the regeneration of the amine scrubbers imposes a ~30–40% load on a power plant and a 60–90% increase in the cost of electricity,[5–7] which introduces an energy penalty. These requirements have a

[a] *Consejo Nacional de Investigaciones Científicas y Técnicas, CONICET – Instituto Balseiro (UNCuyo and CNEA), Centro Atómico Bariloche (CNEA), R8402AGP, S. C. de Bariloche, Río Negro, Argentina. E-mail: gennari@cab.cnea.gov.ar; Fax: +54 294 4445190; Tel: +54 294 4445118*

[b] *European Synchrotron Radiation Facility (ESRF), 71 Avenue des Martyrs, 3800 Grenoble, France*

[c] *Instituto de Investigaciones en Tecnología Química (INTEQUI-CONICET), Almirante Brown 907, San Luis, Argentina*

† Electronic supplementary information (ESI) available: Fig. S1–S7 and Table S1. See DOI: 10.1039/c8cp03611j

direct impact on the cost and currently constitute an incentive for the development of next generation capture materials, in the search of a lower energy cost and greater efficiency.[5–7]

The use of alternative sorbents for CO_2 capture, such as lithium-based silicates, has been investigated in the past years.[8–27] Thermodynamic calculations showed that SiO_2-rich lithium silicates such as Li_2SiO_3, $Li_2Si_2O_5$ and $Li_2Si_3O_7$ could absorb CO_2 at even lower temperatures.[18] These studies also allowed determining the trend of the maximum carbonation temperature at which different lithium silicates capture CO_2, being $Li_8SiO_6 > Li_4SiO_4 > Li_2SiO_3$. In particular, Li_4SiO_4 is one of the most attractive lithium silicates due to its high capture capacity (0.36 g CO_2 per g), high selectivity to CO_2 with respect to other gases and relatively low costs of production.[8–17] Generally, Li_4SiO_4 is synthesized by the solid state technique or ceramic process, using Li_2CO_3 and SiO_2 as reactants:

$$2Li_2CO_3(s) + SiO_2(s) \leftrightarrow Li_4SiO_4(s) + 2CO_2(g) \quad (1)$$

Among the first studies using this synthesis procedure, Pfeiffer *et al.*[28] calcined at 900 °C for 4 h a milled mixture of lithium carbonate and amorphous silica gel. Kato *et al.*[8] mixed in a mortar Li_2CO_3 and SiO_2 and after that the mixture was thermally treated at 1000 °C for 8 h. Other researchers[10,19] prepared Li_4SiO_4 by thermal treatment of the Li_2CO_3–SiO_2 mixture at 900–950 °C for 2–4 h, using different reagent grade precursors of SiO_2. Recently, a detailed study on the effect of the heating rate, thermal temperature and time on the synthesis of Li_4SiO_4 from different Li_2CO_3–SiO_2 mixtures was performed.[27] Complete conversion to Li_4SiO_4 was reached at 900 °C, with a maximum CO_2 uptake of 20% using 0.92 CO_2 partial pressure. However, there are no studies on the formation reaction pathway of Li_4SiO_4 by a solid state method and its relation with other SiO_2-rich lithium silicates. With the aim to reduce costs in an industrial process, the synthesis of Li_4SiO_4 from inexpensive porous diatomite or fly ash as a silicon source was also explored by a solid state synthesis.[12,15,20] The results showed that the sorption capacity was dependent on the carbonate : silica ratio used in the sorbent synthesis. Improved experimental conditions allowed to obtain CO_2 capacities close to that of pure Li_4SiO_4, although these values usually decreased with increasing cycle number.[12] In the case of the Li precursor, Li_2CO_3 was mainly selected as the reactant due to its stability during handling in an air atmosphere.[8–17,21,22] Considering that the geological resources of lithium in the world are limited, the production of binary Na–Li orthosilicate based sorbents was previously studied to decrease the associated costs.[15,29] However, in this work, Li_2CO_3 was preferred because of its high availability in the North of Argentina, where it is produced from natural brines.[30]

To be competitive on a large scale, in addition to high CO_2 capacity and selectivity, Li_4SiO_4 has to possess high stability at elevated temperatures and to be regenerable with fast sorption/desorption kinetics.[8,11,13–18,25,27] The CO_2 capture and desorption processes of Li_4SiO_4 can be represented by the following reversible reaction:

$$Li_4SiO_4(s) + CO_2(g) \leftrightarrow Li_2SiO_3(s) + Li_2CO_3(s) \quad (2)$$

where the reaction enthalpy is $\sim$141 kJ mol^{-1}. The original Li_4SiO_4 is regenerated by heating the carbonate beyond the carbonation temperature. Although high temperature operation is an attractive property of Li_4SiO_4 to avoid lowering the temperature of the exhaust gas stream from the power plant, the absorbent has to keep good sorption capacity, durability and cyclic stability. One important obstacle for the application of Li_4SiO_4 is the kinetic limitations during CO_2 capture, which determine the CO_2 capacity and reversibility, *i.e.*, the reversible formation of Li_4SiO_4 from Li_2CO_3 and Li_2SiO_3.

Different models have been proposed to evaluate the carbonation kinetics. Pfeiffer *et al.* described the absorption process as a two stage reaction. First, a rapid CO_2 chemisorption stage where an external shell of Li_2CO_3 and Li_2SiO_3 is formed. After that step, a slower ion-diffusion controlled stage where both Li^+ and O^{2-} have to diffuse through the product layer to the surface and then react with CO_2. The model assumes that the whole reaction is controlled by the diffusion process. Under this description, a mathematical treatment of the experimental results was made using a double exponential model,[11,13] obtaining in general a good fitting. Rusten *et al.* mentioned that none of the traditional models, like the shrinking core model, shows a satisfactory fit of the experimental data.[31] They used the general expression $F(x) = (1 - x)^n$, with n equal to 2 giving the best fit to the data. The formulation does not explain the CO_2 capture mechanism, but indicates that the rate-limiting step changes with the progress of the reaction. In a recent work, Qi *et al.* proposed a combination of the double-shell model with the Avrami–Erofeev kinetic model to fit the CO_2 capture and desorption processes.[32] The physical description includes the formation of Li_2CO_3 and Li_2SiO_3 nuclei when CO_2 reacts with the surface of Li_4SiO_4 particles. These nuclei grow to form a double shell covering the unreacted Li_4SiO_4. Subsequently, CO_2 diffuses across the external Li_2CO_3 layer to react with the Li^+ and O^{2-} ions, which have moved from the unreacted Li_4SiO_4 along the Li_2SiO_3 barrier.

In this work, Li_2CO_3 and SiO_2 were selected as precursors for the synthesis of Li_4SiO_4 due to their stability, availability and local price. With the aim to develop a synthesis procedure to be used in large scale production of Li_4SiO_4, the conventional solid-state synthesis was modified by introducing a milling step to reduce the temperature and time required during the thermal treatment. The formation of Li_4SiO_4 at a low temperature during the thermal treatment from the as-milled Li_2CO_3–SiO_2 mixture as well as the carbonation reaction of Li_4SiO_4 was studied using thermodynamic calculations, thermal analysis, TG measurements, microstructural analysis and both *ex situ* X-ray diffraction and *in situ* time resolved synchrotron X-ray diffraction measurements. New insights into the mechanism of both the formation and the carbonation of Li_4SiO_4 are provided.

2. Experimental

2.1 Synthesis of the composites: thermodynamic calculations

The equilibrium composition for the Li–Si–O system with dissimilar Li_2CO_3–SiO_2 starting ratios as a function of the

temperature was calculated using HSC Chemistry (HSC Chemistry for Windows, 6.1 version).[33] The program determines the most stable species combination and the phase composition where the Gibbs free energy of the system reaches its minimum at constant pressure and temperature, assuming that the condensed phases are pure. The results were obtained for a reacting system composed of 1 (or 2) kmol of Li_2CO_3 and 1 kmol of SiO_2 in air (N_2 = 78 kmol and O_2 = 21 kmol O_2).

2.2 Material preparation

Lithium carbonate (Biopack, 97%) and silica (Sigma, high purity grade) were selected as starting materials. Mixtures of Li_2CO_3–SiO_2 with 1 : 1 and 2 : 1 molar ratios were mechanically milled (MM) in a planetary ball mill (Fritsch Pulverisette P6) for different times at room temperature under an air atmosphere. The selected milling conditions were a ball to powder ratio of 50 : 1 and 400 rpm. After mechanical processing, the samples were annealed with a ramp of 5 °C min^{-1} at temperatures between 500 and 800 °C for different times from 1 h to 24 h. A scheme of the synthesis procedure is shown in Fig. S1 (ESI†). Lithium volatilization at high temperature was reduced due to the presence of SiO_2 homogeneously mixed with Li_2CO_3. As a reference, Li_2CO_3 and SiO_2 with 2 : 1 molar ratio were physically mixed (PM) using a V-shaped drum mixer.

2.3 Characterization techniques

Ex situ X-ray powder diffraction (XRPD, Bruker D8 Advance) measurements with CuKα radiation were used to identify structural changes in samples during the synthesis procedure and thermal treatments. Scans were collected in the (2θ) range of 10–80° with a scan rate of 1.2° min^{-1}, using a voltage of 40 kV and an electric current of 40 mA. The thermal behaviour of the as-milled Li_2CO_3 : SiO_2 mixtures (1 : 1 and 2 : 1 ratio) was monitored with a Shimadzu DTA/TG thermal analyzer in an air atmosphere and a heating rate of 10 °C min^{-1} from room temperature to 800 °C. N_2 adsorption isotherms were obtained on a Micromeritics ASAP 2020 analyzer at −196 °C. Prior to the analysis, 0.2 g of sample was evacuated at 350 °C overnight. Surface area and pore distribution were obtained by applying the BET method.

Dynamic and isothermal CO_2 capture measurements were performed with a thermogravimetric instrument (TG-HP50, TA Instruments). The sample was dynamically heated from room temperature to 800 °C at a heating rate of 5 °C min^{-1} using a CO_2 flow rate of 50 cm^3 min^{-1} (STP). For the isothermal analysis, the samples were first heated from room temperature under a He flow to the selected temperature (700 °C) and after that the flow gas was switched from He to CO_2. Then, an isothermal period for the carbonation was maintained. Reference tests under isothermal and non-isothermal conditions were performed to correct for the buoyancy effect. After the CO_2 capture process, the morphology of the powders was studied by scanning electron microscopy (SEM, SEM-FEI Inspect S50 and SEM-FIB, Zeiss, Crossbeam 340). All powder samples were covered with gold to improve the electrical conductivity of the ceramics.

The synthesis and carbonation of Li_4SiO_4 were followed by *in situ* synchrotron radiation X-ray powder diffraction (SR-XRPD) analysis. The samples were placed in a 0.9 mm diameter quartz capillary, which was open at both ends. The capillary was horizontally placed on top of a gas blower that enabled heating and cooling in the temperature range (25–775 °C). The inlet of the capillary was connected to three mass flow controllers that allowed the feed of synthetic air, N_2 and CO_2. During the synthesis, the as-milled $2Li_2CO_3$–SiO_2 mixture was heated from room temperature to 615 °C at a rate of 5 °C min^{-1} under 10 mL min^{-1} flow of synthetic air. For CO_2 sorption experiments, the sample was subjected to a 10 mL min^{-1} flow of CO_2 : N_2 (50 : 50) and heated from room temperature to 645 °C. The temperature was kept constant for 2 h and then the heating ramp was continued until 750 °C. *In situ* synchrotron powder X-ray diffraction measurements were performed at the beamline ID31 of the European Synchrotron Radiation Facility (ESRF). The data were acquired using a 2D Perkin Elmer detector, the wavelength was 0.1771 Å and the beam size was 0.6 × 0.6 mm. The acquisition time for each XRPD pattern was 2 s and the time resolution was 1 pattern each 30 s. The data were integrated using the pyFAI package and the Rietveld analysis was performed using Fullprof suite software.[34]

3. Results and discussion

3.1 Mechanism of Li_2SiO_3 and Li_4SiO_4 formation from Li_2CO_3–SiO_2 mixtures

Thermodynamic calculations were performed to determine the equilibrium composition of the Li_2CO_3–SiO_2 system based on the Gibbs energy minimization method.[33] The evolution of the different species was estimated in an air atmosphere (constant pressure = 1 bar) and as a function of temperature. The results obtained are shown in Fig. 1 for the Li_2CO_3–SiO_2 mixtures with 1 : 1 (Fig. 1A) and 2 : 1 (Fig. 1B) starting compositions. The overall chemical reaction at high temperature for each composition of the Li_2CO_3–SiO_2 system can be expressed as:

$$Li_2CO_3(s) + SiO_2(s) \rightarrow Li_2SiO_3(s) + CO_2(g) \quad (3)$$

$$2Li_2CO_3(s) + SiO_2(s) \rightarrow Li_4SiO_4(s) + 2CO_2(g) \quad (1)$$

From Fig. 1A and B (1 : 1 and 2 : 1 compositions, respectively), it is possible to infer that the formation of Li_2SiO_3 and Li_4SiO_4 starts at about 100 °C and 400 °C, respectively, by annealing of the starting mixture in air. The only gaseous product predicted is CO_2. In addition, for both compositions, the formation of $Li_2Si_2O_5$ as an intermediate compound from the starting reactants is expected:

$$Li_2CO_3(s) + 2SiO_2(s) \rightarrow Li_2Si_2O_5(s) + CO_2(g) \quad (4)$$

Reaction (4) occurs in a specific interval of temperature that depends on the initial Li_2CO_3–SiO_2 composition. As temperature increases, $Li_2Si_2O_5$ is consumed to produce more Li_2SiO_3 according to reaction (5):

$$Li_2Si_2O_5(s) + Li_2CO_3\ (s) \rightarrow 2Li_2SiO_3\ (s) + CO_2\ (g) \quad (5)$$

Moreover, for the 1 : 1 composition, Li_2SiO_3 is the main component in the solid reaction products at about 500 °C.

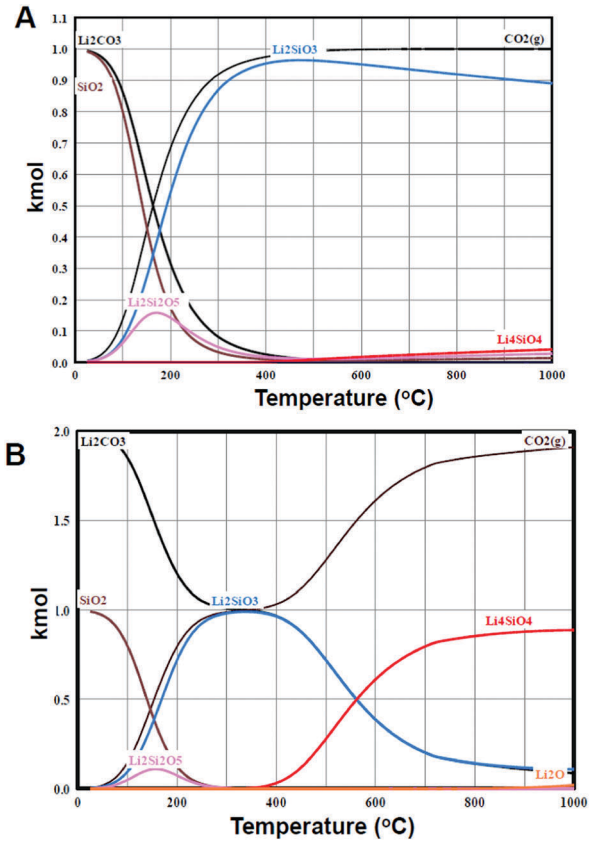

Fig. 1 Equilibrium composition of the Li_2CO_3–SiO_2 system with (A) 1 : 1 and (B) 2 : 1 molar ratios.

As the temperature increases, Li_2SiO_3 coexists with minor amounts of Li_4SiO_4. In the case of the $2Li_2CO_3$–SiO_2 mixture (Fig. 1B), the equilibrium composition suggests that the mechanism of Li_4SiO_4 formation involves a two step process: first, the formation of Li_2SiO_3 according to reaction (3) up to 350 °C, followed by the reaction between Li_2SiO_3 and the remnant Li_2CO_3 as temperature increases.

$$Li_2SiO_3(s) + Li_2CO_3(s) \rightarrow Li_4SiO_4(s) + CO_2(g) \quad (6)$$

The equilibrium composition predicts that Li_4SiO_4 is the main solid product at 800 °C. It exists with minor amounts of Li_2SiO_3 at high temperature (800–1000 °C) in a closed system (reaction (6)), in the presence of Li_2O and CO_2 due to the expression (7):[35]

$$Li_2CO_3(s) \leftrightarrow Li_2O(s) + CO_2(g) \quad (7)$$

In order to analyze the influence of the starting composition of the as-milled Li_2CO_3–SiO_2 mixture on the synthesis of Li_2SiO_3 and Li_4SiO_4, thermal analysis using a TG–DTA technique was performed. The curves obtained are shown in Fig. 2. For comparison, the curves corresponding to the as-milled Li_2CO_3 and SiO_2 starting materials as well as physically mixed $2Li_2CO_3$–SiO_2 mixture are presented. The TG curves of the as-milled Li_2CO_3–SiO_2 mixtures (compositions 1 : 1 and 2 : 1, Fig. 2A) show a progressive weight loss from room temperature

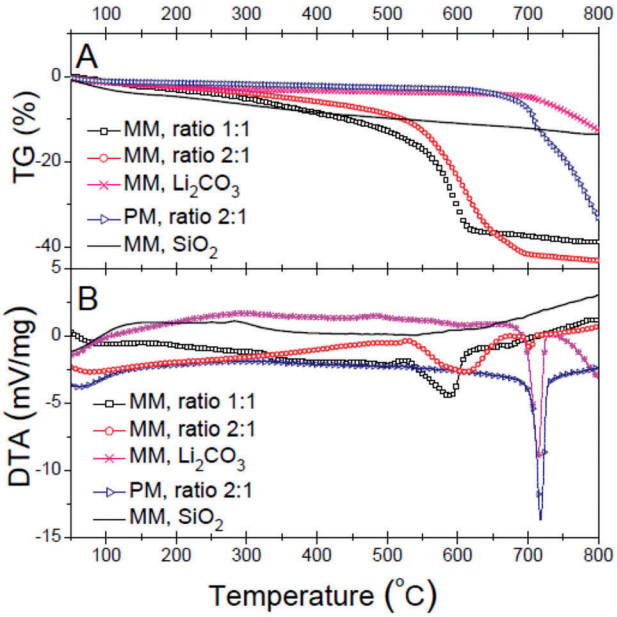

Fig. 2 TG (A) and DTA (B) curves of mechanically milled (MM) Li_2CO_3–SiO_2 mixtures with 1 : 1 and 2 : 1 ratios; $2Li_2CO_3$–SiO_2 powders physically mixed (PM) and as-milled Li_2CO_3 and SiO_2.

up to about 500 °C. After that, a sharp weight loss is observed. The whole weight loss measured up to 800 °C was about 39% and 43% for the 1 : 1 and 2 : 1 compositions, respectively. However, the theoretical values expected according to reactions (1) and (2) are 32.8% and 42.3%, respectively. The differences can be ascribed mainly to pre-adsorbed water and possibly other volatile contamination of the starting materials, which was released during heating. In fact, MM SiO_2 evidences an important weight loss over the whole temperature range, being about 10% at 500 °C. On the other hand, PM $2Li_2CO_3$–SiO_2 does not show a weight change up to 600 °C but undergoes 38% weight loss at 800 °C. By comparison of these measurements, it is clear that the adsorption of water and other species was favoured by milling, a processing method of solids that enhances the surface area of the samples. Considering that the weight loss measured at 400 °C for the as-milled Li_2CO_3–SiO_2 mixtures was about 9% and 6% for the 1 : 1 and 2 : 1 compositions, respectively, the experimental values approach the theoretical ones as stated by reactions (3) and (1). However, the differences between these values after correction for water adsorption indicate that the reaction between Li_2CO_3 and SiO_2 was incomplete during the heating ramp up to 800 °C.

The different thermal behaviours displayed in Fig. 2B confirm the previous interpretation: two different temperature regions can be identified on heating. From room temperature to about 500 °C, the DTA signal for all samples does not show a clear thermal change, independently of the presence or not of the adsorbed species. After that, a chemical process starts that is endothermic and has an associated sharp weight loss. For the Li_2CO_3–SiO_2 mixtures, this process can be mainly attributed to the CO_2 release from Li_2CO_3 due to the formation of Li_2SiO_3 according to reaction (3) and promoted by both the ball milling

and the presence of SiO_2. In the case of the 2 : 1 composition, reactions (1), (3) and (6) are thermodynamically favourable in this range of temperature to produce Li_4SiO_4 as the final product. Moreover, an extra endothermic event was detected at 705 °C for the 2 : 1 composition. A similar endothermic peak at 715 °C was found for the physically mixed sample and for pure MM Li_2CO_3. Then, this event can be ascribed to the melting point of the unreacted Li_2CO_3. Above this temperature, the reactivity between liquid Li_2CO_3 and Li_2SiO_3 (reaction (6)) or residual SiO_2 (reaction (3)) is improved to additionally form Li_4SiO_4.

With the aim to correlate the equilibrium composition (Fig. 1B) and the thermal behaviour of the as-milled $2Li_2CO_3$–SiO_2 mixture (Fig. 2), the progression of the phases under heating in air was followed by time-resolved synchrotron powder X-ray diffraction studies. Fig. 3 shows the evolution of the diffractograms collected during heating of the as-milled $2Li_2CO_3$–SiO_2 mixture in the temperature range from 40 °C to 615 °C under air flow. Fig. S2 (ESI†) displays the contour plot of the acquired *in situ* SR-XRPD data during the synthesis of Li_4SiO_4 under synthetic air as a function of time and temperature (heating rate 5 °C min^{-1} up to 615 °C). At temperatures lower than 400 °C, no evidence of structural changes was detected in the sample. As temperature increases, the formation of Li_2SiO_3 is clearly observed at 490 °C. Afterwards, the most intense peaks of Li_4SiO_4 appeared and coexisted with those of Li_2SiO_3. Further increasing the temperature up to 550 °C induces the complete consumption of Li_2SiO_3 as well as the progressive production of Li_4SiO_4. At 615 °C, the phases identified were Li_4SiO_4 and unreacted Li_2CO_3. An additional temperature increase is required to complete the Li_4SiO_4 production. From this *in situ* study, it is possible to confirm that Li_2SiO_3 is an intermediate compound during the synthesis of Li_4SiO_4 and that it is formed and consumed in a specific temperature range. This result is in agreement with the thermodynamic prediction and corroborates the fact that the two mechanisms of Li_4SiO_4 formation contribute to the endothermic peak obtained by DTA: the formation of Li_2SiO_3 as an intermediate (reactions (2) and (6)) and the direct reaction between Li_2CO_3 and SiO_2 (reaction (1)). Moreover, no evidence of the appearance of the $Li_2Si_2O_5$ phase was detected under heating, in contrast with the thermodynamic prediction, probably due to kinetics restrictions. The minor differences between the reaction temperatures determined using TG–DTA and *in situ* X-ray diffraction measurements can be attributed to the different experimental set-up, especially the dynamic flow conditions.

To next evaluate the CO_2 capture performance of the thermally treated Li_2CO_3–SiO_2 mixtures (1 : 1 and 2 : 1), the effect of different times (5 h and 24 h) and temperatures (500, 600, and 800 °C) on the formation of Li_2SiO_3 and Li_4SiO_4 was studied. The *ex situ* XRPD patterns obtained at variable temperatures and times are shown in Fig. S3 (ESI†) and Fig. 4. As a relevant result, 5 h of heating at 600 °C of the as-milled Li_2CO_3–SiO_2 mixtures favours the formation of Li_2SiO_3 and Li_4SiO_4 as the main products for the 1 : 1 and 2 : 1 ratios, respectively (Fig. S3B, ESI† and Fig. 4B). This sharp reduction in the formation temperature of Li_2SiO_3 and Li_4SiO_4 (500 °C) in comparison with both the conventional solid state route (higher than 800 °C)[8,10,19,27,28] and the physical mixting of the powders (Fig. 4B) demonstrates the important role of the ball milling step in the synthesis procedure. It is known that mechanical milling favours the refinement of the powder microstructure and generates surface/bulk defects, improving posterior reactivity of the components, especially for ceramic materials.[36,37] In the case of the Li_2CO_3–SiO_2 mixture, minor amounts of Li_4SiO_4 were detected at 600 °C (5 h and 24 h, Fig. S3, ESI†) and found to coexist with the desired product Li_2SiO_3 even after heating at 800 °C for 5 h, in agreement with thermodynamic calculations (Fig. 1).

For the composition $2Li_2CO_3$–SiO_2, the majority of the Li_4SiO_4 formation was observed after annealing at 600 °C for 5 h and 24 h (Fig. 4A and B, respectively); however, the three main reflections of Li_2CO_3 were clearly identified. Moreover, heating for 5 h at 800 °C induces the formation of Li_4SiO_4 (94 wt%) and only a weak

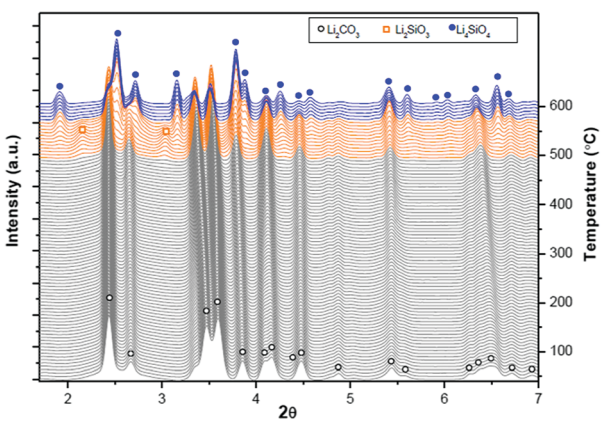

Fig. 3 *In situ* SR-XRPD patterns collected during the synthesis of Li_4SiO_4.

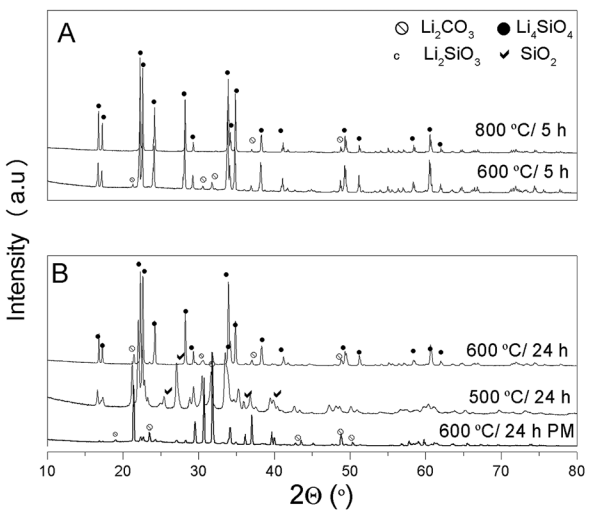

Fig. 4 *Ex situ* XRPD patterns of Li_4SiO_4 formation from the as-milled $2Li_2CO_3$–SiO_2 mixture: (A) 800 and 600 °C, 5 h; (B) 600 and 500 °C, 24 h (MM and PM).

reflection of Li_2CO_3 was detected (Fig. 4A and Fig. S4, Table S1, ESI†). This result is in agreement with a recent work, where unconverted Li_2CO_3 was detected in all samples prepared at temperatures lower than 900 °C by solid state synthesis.[27] Due to its high Li_4SiO_4 yield, the sample heated at 800 °C for 5 h was selected for further studies.

3.2 CO_2 capture by as-synthesized Li_2SiO_3 and Li_4SiO_4 powders

The powders of Li_2SiO_3 and Li_4SiO_4 produced by milling plus heating at 800 °C for 5 h (XRPD in Fig. 4A and Fig. S4, S3A, ESI†) were evaluated as carbon dioxide absorbents by performing non-isothermal TG measurements. Fig. 5 displays the TG curves for the synthesized Li_2SiO_3 and Li_4SiO_4. It can be seen that Li_2SiO_3 seems to absorb CO_2 at low temperature, reaching about of 3 wt% at 200 °C. Further increasing the temperature does not induce relevant CO_2 capture, with the maximum amount of CO_2 absorbed being about 5 wt% at 800 °C. The carbonation behaviour of Li_2SiO_3 was previously analyzed by different authors,[8,11,18,38] but the results were contradictory. Khomane *et al.*[38] showed that Li_2SiO_3 slowly captures CO_2 up to 580 °C, while a sharp increase was exhibited between 580 °C and 610 °C. After that, release of CO_2 starts beyond 630 °C.

Venegas *et al.*[11] found that the Li_2SiO_3 formed during carbonation of Li_4SiO_4 further reacts with CO_2 to form SiO_2 and Li_2CO_3, enhancing the CO_2 capture properties of Li_4SiO_4. Kato *et al.*[8] showed that no weight increase was observed under CO_2 heating up to 900 °C. They suggested that Li_2SiO_3 can absorb CO_2 at temperatures of less than 250 °C, but the absorption rate is very slow in this temperature range. Recently, a theoretical study predicted that the Li_2O-rich lithium silicates could absorb CO_2 even at low temperatures.[18] It was indicated that the disagreement between prediction and experiment arises due to kinetics restrictions that constrain the capture rates. Our results are coincident with the observation that Li_2SiO_3 could absorb CO_2 at low temperature, but the amount of CO_2 captured is limited by kinetics restrictions. In contrast with Li_2SiO_3, Li_4SiO_4 began to clearly absorb CO_2 at 550 °C and it increases up to 700 °C. A sharp increment in the CO_2 capture occurs at 720 °C, finishing this process at 34% weight change (the theoretical value is 36.7 wt%). In fact, the CO_2 capture process for Li_4SiO_4 can be divided into two clear temperature ranges: the first step from 550 to 700 °C associated with a superficial process; the second one, from 700 to 770 °C, corresponding to the bulk CO_2 diffusion process. The as-synthesized Li_4SiO_4 is able to take up/release CO_2 (inset plot Fig. 5) reversibly, maintaining a CO_2 capacity between 34–35 wt% after at least 10 cycles. However, the carbonation/decarbonation rate decreased after the third cycle with increasing the cycle number. This behaviour is associated with the loss of the Li_4SiO_4 microstructure by sintering, as was previously observed.[12,20]

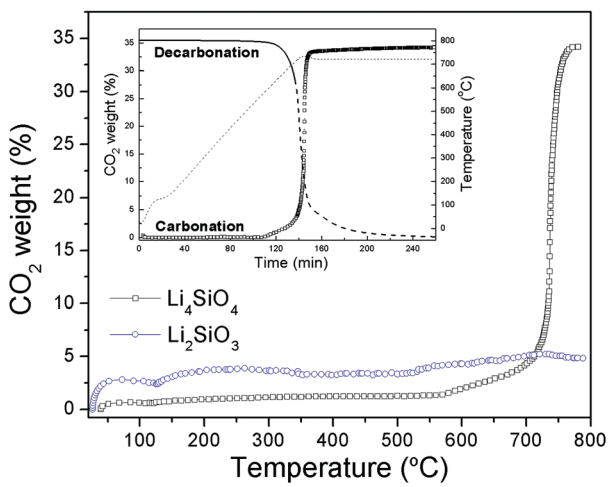

Fig. 5 TG curves of Li_2SiO_3 and Li_4SiO_4 during heating under pure CO_2 flow (ramp 5 °C min^{-1}). Inset plot shows carbonation/decarbonation cycle of Li_4SiO_4 at 720 °C.

The morphological features of the Li_4SiO_4 powders before and after CO_2 capture are shown in Fig. 6A and B, respectively. The original Li_4SiO_4 powders (Fig. 6A) exhibited agglomerates with sizes lower than 50 μm while after CO_2 absorption, the morphology aspect of the material appears entirely different. The carbonate formation leads to the aggregation of powders during the chemisorption step. It can be proposed that the initial carbonate formation at the surface forms a shell around the particles and promotes their coalescence.

Progressively bulk carbonate generation contributes to the development of an aggregated microstructure, as shown in Fig. 6B, where the sintering is evident.

The N_2 adsorption–desorption isotherm for the as-synthesized Li_4SiO_4 powders was obtained to determine their textural characteristics (data not shown). The curve corresponds to a type II isotherm according to the IUPAC classification, and it did not show hysteresis. This behaviour is correlated to nonporous particles and/or dense aggregates of particles. Additionally, the sample surface area was estimated to be about 1 m^2 g^{-1} using the BET model.

3.3 *In situ* synchrotron powder X-ray diffraction studies of Li_4SiO_4 during dynamical carbonation reaction

To focus on the reaction mechanism between Li_4SiO_4 and CO_2, Fig. 7A shows the *in situ* SR-XRPD patterns collected at different temperatures during the whole carbonation process. It can be seen from selected patterns that the carbonation reaction starts at about 410 °C, as can be inferred from the simultaneous

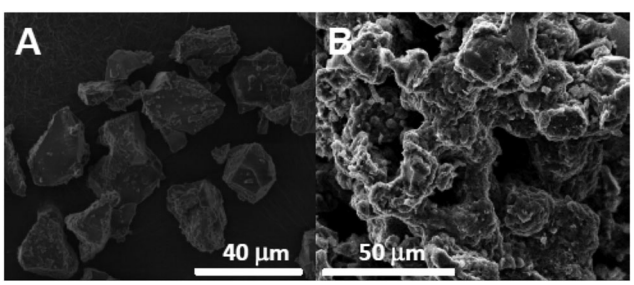

Fig. 6 Secondary electron photographs of the (A) as-synthesized Li_4SiO_4 powders and (B) Li_4SiO_4 powders after dynamic CO_2 capture.

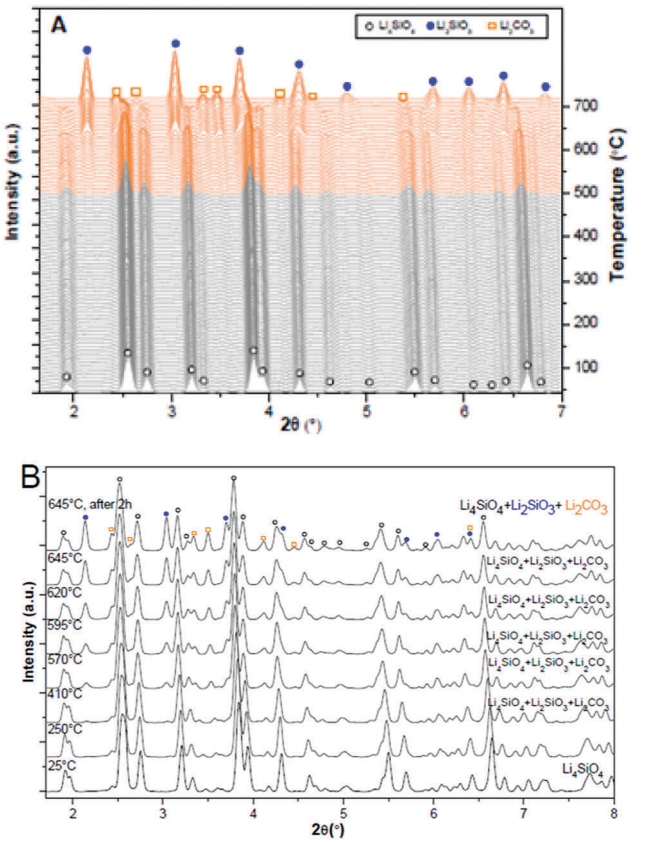

Fig. 7 (A) *In situ* SR-XRPD data collected during the whole carbonation process, and (B) SR-XRPD patterns corresponding to different temperatures during carbonation. The phases present at each temperature are indicated within the graph.

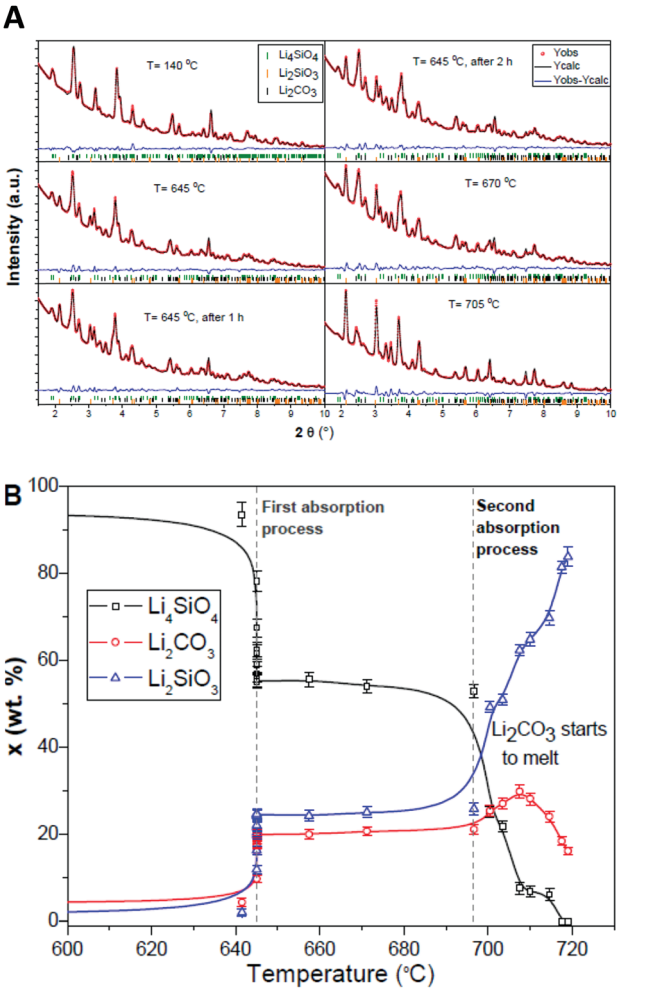

Fig. 8 (A) SR-XRPD patterns collected during Li_4SiO_4 carbonation. Red circles correspond to experimental data, the black line corresponds to the data calculated from the Rietveld analysis and the blue line is the difference between experimental data and fitted data. (B) Evolution of the mass fraction of Li_4SiO_4 (black square), Li_2CO_3 (red circle) and Li_2SiO_3 (blue triangle) against temperature during carbonation.

detection of Li_2SiO_3 and Li_2CO_3 (Fig. 7B and Fig. S5, ESI†). Besides, the CO_2 capture is significant at 645 °C and after 2 h at this temperature, the reaction was not complete. Moreover, further heating of the material to the final temperature (715 °C) resulted in the completion of the reaction. This fact can be deduced from the disappearance of the peaks belonging to Li_4SiO_4 and the increasing amount of Li_2SiO_3. In the case of Li_2CO_3, a progressive decreasing of the crystalline fraction with the temperature increase was determined as in relation to different processes: the Li_2CO_3 melting, and volatilization and/or its simultaneous partial decomposition under flow.[35] In fact, measurements obtained after cooling the system down showed the peaks corresponding to Li_2CO_3, indicating, indeed, partial Li_2CO_3 recrystallization. These results demonstrate the absence of secondary reactions and confirm that the carbonation process of Li_4SiO_4 occurs according to reaction (2), forming Li_2SiO_3 and Li_2CO_3.

Fig. 8A shows the SR-XRPD patterns fitted using Rietveld refinement at different stages of the carbonation reaction of Li_4SiO_4. Based on these results, the amount of different phases at each temperature was calculated. In Fig. 8B, the mass fractions (in wt%) of Li_4SiO_4, Li_2CO_3 and Li_2SiO_3 are shown at several intermediate temperatures as calculated from the Rietveld analyses of the experimental data. It is possible to observe that the system absorbed CO_2 in two processes. The first one, which started at about 410 °C, continues until the second absorption stage, which continues until the full absorption up to 645 °C, increasing the amount of Li_2CO_3 and Li_2SiO_3 formed. However, after 2 h at this temperature, it is not possible to complete the reaction and an equilibrium state was reached with a reacted fraction of Li_4SiO_4 of around 40%. From the observed diffractograms, in order to achieve complete transformation, a temperature of 715 °C is required. Also, from Fig. 8B, it is possible to deduce that the two processes occurring at the two different temperatures are different in nature.

In fact, after the first stage, the system does not continue absorbing CO_2 immediately after a temperature increment, as would be expected from an absorption mechanism, but enters into a plateau with a nearly constant amount of CO_2 absorbed. This is indicative of a surface reaction, where Li_2CO_3 forms a layer. Once reaching approximately 696 °C, the system enters

into the second absorption stage, which continues until the full absorption. The second small plateau observed at around 708 °C is actually an artefact caused by the beginning of the melting process of Li_2CO_3, which causes an apparent increment in the fraction of Li_4SiO_4 present.

In order to understand the first step in the carbonation process of Li_4SiO_4, two different TG measurements were performed using isothermal and non-isothermal conditions. When carbonation was measured under dynamic conditions from room temperature to 700 °C (Fig. 9A), the general behaviour was as shown in Fig. 5. Two regions can be identified. The first region was characterized by a fast weight gain, where 4 wt% of CO_2 is captured under non-isothermal conditions (between 560 °C and 700 °C) and continuing up to 8.5 wt% under isothermal conditions (700 °C) with a carbonation rate of 0.29 wt% min^{-1} (at 6.5 wt%). The second region occurs completely at 700 °C and is distinguished by a slower carbonation rate (0.04 wt% min^{-1} at 11 wt%), which reaches about 16 wt% after 6.7 h. Moreover, carbonation of Li_4SiO_4 under isothermal conditions at 700 °C displays an unexpected behaviour: the final CO_2 capture was only 6 wt%, with a fast stage at the beginning followed by a decrease in the reaction rate during the second stage. In fact, the carbonation rate at each stage is about three to four times lower than those obtained for dynamic conditions. Considering that the experimental set up

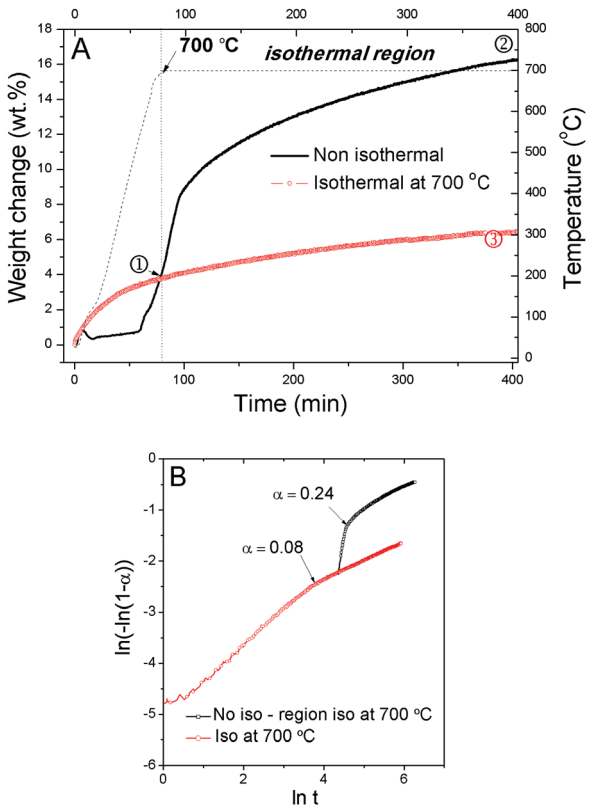

Fig. 9 (A) TG curves of Li_4SiO_4 obtained during: (a) non-isothermal heating up to 700 °C under pure CO_2 flow (5 °C min^{-1}); (b) heating to 700 °C under He flow and change to CO_2 flow. (B) Fit of the CO_2 sorption kinetic experimental data.

and CO_2 flow conditions are the same in both measurements, a different controlling mechanism seems to influence the kinetics of isothermal measurement that restricts posterior carbonation.

The Avrami–Erofeev model was recently applied for the carbonation of Li_4SiO_4 and it was demonstrated that it is the most adequate for the CO_2 sorption process within a wide temperature range.[32] In particular, this model can describe the rapid reaction stage at the beginning generally neglected in the double exponential model or shrinking core model. Fig. 9B represents the $\ln(-\ln(1-\alpha))$ *versus* $\ln t$ plot of the experimental data shown in Fig. 9A, at 700 °C, for the isothermal and non-isothermal runs. Both curves show inflexion points at low conversions: for the isothermal run, it corresponds with a Li_4SiO_4 conversion of about 0.1; for the non-isothermal run in the isothermal region at 700 °C, the inflexion point was observed at 0.24 of conversion.

From the linear fits of $\ln(-\ln(1-\alpha))$ *versus* $\ln t$ for the two stages, the n values for each stage were obtained (Fig. 9B). In the first stage, the slope for the non-isothermal run was larger than 1 (near to 4), whereas for the isothermal measurement, it was lower than 1 (about 0.7). This result denotes that in the first case, the reaction is controlled by the rate of formation and growth of the reaction (point 1, Fig. 9) products while in the second case, the process is under diffusion control. This is evidence that a different control operating from the beginning of Li_2CO_3 formation neglects further carbonation due to diffusion control in the isothermal measurement. Moreover, in the second stage, the slopes of both runs are approximately 0.4, which strongly suggests that the CO_2 sorption is under diffusion control. Then, for the non-isothermal measurement in the isothermal region, a change in the controlling step is operating, while the whole isothermal measurement is under diffusion control.

Microstructural information of Li_4SiO_4 during the carbonation process was obtained by SEM analysis at different CO_2 weight changes (as indicated in Fig. 9A, points 1, 2 and 3). To compare, Fig. S6 (ESI†) shows a detail of an agglomerate of as-synthesized Li_4SiO_4, which is characterized by straight edges and a smooth surface. A secondary electron image and the elemental mapping of Li_4SiO_4 after 4 wt% carbonation under non-isothermal measurement are shown in Fig. 10. The oxygen element was taken as a reference because it is present both in Li_2CO_3 and Li_2SiO_3/Li_4SiO_4. Its absence indicates a region with a different topology. By comparison, the C is homogeneously distributed in the material, suggesting the presence of Li_2CO_3 on the whole surface. Moreover, some zones with high C concentration were identified and related with the small Li_2CO_3 crystals of less than 2 μm (see SEM image). In these zones, Si element is practically undetected. However, Si distribution evidences the presence of Li_4SiO_4 on the near surface, which is available for further CO_2 interaction.

Fig. 11 displays the morphology and the chemical mapping of Li_4SiO_4 after 6 wt% carbonation under isothermal conditions (point 3, Fig. 9). The SEM image shows the presence of crystals of about 10 μm (indicated by arrows) due to Li_2CO_3, as indicated by C mapping. Si element is practically undetectable in these crystals

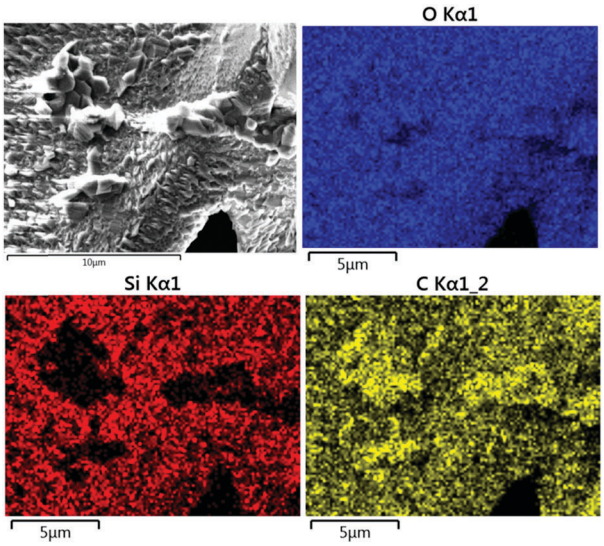

Fig. 10 SEM micrograph and chemical mapping of Li_4SiO_4 after 4 wt% CO_2 capture under non-isothermal conditions (point 1, Fig. 9).

and its distribution is clearly non homogeneous. These observations reinforce the idea that a carbonate shell was formed over the surface of the Li_4SiO_4 particles leading to slower CO_2 sorption and the controlling step is the diffusion of lithium through the double layer. Fig. S7 (ESI†) shows the morphology and elemental mapping after 16 wt% carbonation (non-isothermal run, point 2 in Fig. 9). The C and Si distributions evidence the presence of Li_2CO_3 crystals, with sizes similar to those observed after 6 wt% carbonation under isothermal conditions (Fig. 11). As an interesting result, even after 16 wt% CO_2 capture, some regions show the presence of Si in the near surface of the powder.

The experimental information provided in Fig. 9–11 evidences the relation between the mechanism of Li_2CO_3 layer formation,

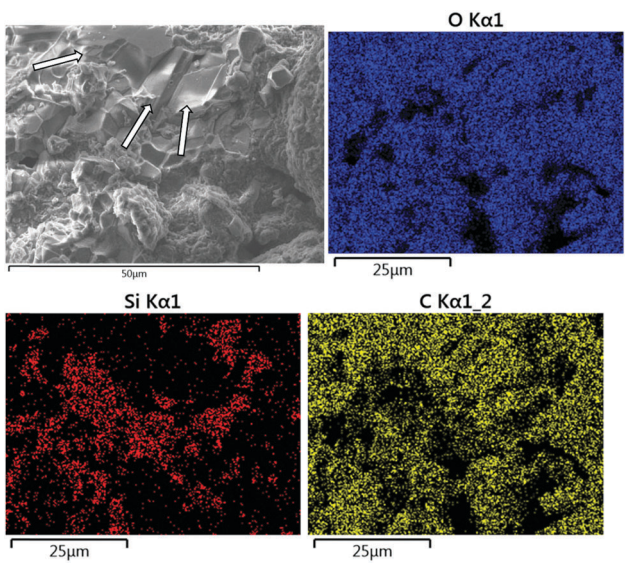

Fig. 11 SEM micrograph and chemical mapping of Li_4SiO_4 after 6 wt% CO_2 capture under isothermal conditions (point 3, Fig. 9).

its microstructure and the CO_2 capture capacity reached at a fixed temperature. The isothermal carbonation allows the formation of a higher amount of Li_2CO_3 nuclei that create a thin carbonate shell. Under this panorama, Li_2CO_3 covers the Li_4SiO_4 particle surface, which reduces the availability of active surface for additional carbonation. The CO_2 diffusion through this layer from the surface to the bulk is the limiting step from the beginning and further carbonation is restricted as the reaction progresses. In contrast, during non-isothermal measurement, the generation of a lower quantity of Li_2CO_3 nuclei leads to retardation of the double shell formation. Then, the rate of formation and growth of the Li_2CO_3 remains the reaction controlling step up to much higher conversion values. These results provide new insights for the understanding of the CO_2 interaction with Li_4SiO_4.

4. Conclusions

In this work, the formation and carbonation of Li_4SiO_4 were examined using *in situ* synchrotron radiation powder X-ray diffraction combined with thermal analysis (DTA and TG), microscopic observations and thermodynamic calculations. Due to the relevance of Li_2SiO_3 compound in the carbonation/decarbonation reversible process, its formation and reactivity under CO_2 flow were also evaluated.

The synthesis of Li_2SiO_3 and Li_4SiO_4 was performed by a two step process: milling of the Li_2CO_3–SiO_2 mixture (with 1 : 1 and 2 : 1 ratios, respectively) followed by annealing at different temperatures. The mechanical milling improves the reactivity between Li_2CO_3 and SiO_2, allowing the formation of Li_2SiO_3 and Li_4SiO_4 even at 600 °C. In fact, 94% Li_4SiO_4 was obtained after heating at 800 °C for 5 h. It was demonstrated that the formation pathway of Li_4SiO_4 involves Li_2SiO_3 as an intermediate compound, in agreement with thermodynamic calculations. However, in spite of thermodynamic predictions, the $Li_2Si_2O_5$ formation was not detected at intermediate temperatures, possibly due to kinetic restrictions.

The as-produced Li_2SiO_3 powders absorb CO_2 at low temperatures, about 3 wt% at 200 °C, and they present a limited final capacity of 5 wt% at 800 °C. In opposition, the as-synthesized Li_4SiO_4 showed a significant CO_2 uptake performance (34–35 wt%) within the temperature range of 550–730 °C and a good regenerability at 720 °C. By performing dynamical measurements at temperatures lower than the melting point of Li_2CO_3, it was observed that non-isothermal heating under CO_2 from room temperature up to 700 °C favours the formation of a lower quantity of Li_2CO_3 nuclei, delaying the double shell formation. Thus, the carbonation rate is controlled by the formation and growth of the Li_2CO_3 nuclei, extending this step to a higher CO_2 capture capacity. Under isothermal conditions at high temperatures such as 700 °C, the carbonation reaction promotes the formation of a higher amount of Li_2CO_3 nuclei, which collapse among themselves forming a layer of Li_2CO_3. This layer is responsible for practically blocking the access to the Li_4SiO_4 particle surface and delaying further CO_2 capture

capacity. Then, CO_2 diffusion from the surface across the Li_2CO_3 layer to the bulk is the limiting step of the carbonation reaction from the beginning of the process. This work provides new insights on the mechanism of both the formation and carbonation of Li_4SiO_4, which can impact on the performance of Li_4SiO_4.

Conflicts of interest

There are no conflicts to declare.

Acknowledgements

The financial support of the CONICET (the National Council of Scientific and Technological Research), CNEA (the National Commission of Atomic Energy) and ANPCyT (National Agency of Scientific and Technological Promotion) is gratefully acknowledged. The authors thank Afra Fernández Zuvich, Alberto Baruj and Bernardo Pentke for the SEM micrographs. The authors also thank the ESRF for in-house beam time allocation. F. C. G. gratefully acknowledges the financial support from L'Oréal-UNESCO National Award for Women in Science, in collaboration with CONICET (2016).

Notes and references

1 *IPCC: Climate Change: Synthesis Report*, ed. R. K. Pachauri and L. A. Meyer, Geneva, *Switzerland*, 2014, p. 151.
2 D. D'Alessandro, B. Smit and J. Long, *Angew. Chem., Int. Ed.*, 2010, **49**, 6058–6082.
3 N. MacDowell, N. Florin, A. Buchard, J. Hallett, A. Galindo, G. Jackson, C. S. Adjiman, C. K. Williams, N. Shah and P. Fennell, *Energy Environ. Sci.*, 2010, **3**, 1645–1669.
4 M. K. Mondal, H. K. Balsora and P. Varshney, *Energy*, 2012, **4**, 6431–6441.
5 A. S. Bhown, *Energy Procedia*, 2014, **63**, 542–549.
6 Electric Power Research Institute, Program on Technology Innovation: Post combustion CO_2 Capture Technology Development, Electric Power Research Institute, Palo Alto, 2008.
7 R. S. Haszeldine, *Science*, 2009, **325**, 1647–1652.
8 M. Kato, S. Yoshikawa and K. Nakagawa, *J. Mater. Sci. Lett.*, 2002, **21**, 485–487.
9 K. Essaki, M. Kato and H. Uemoto, *J. Mater. Sci.*, 2005, **18**, 5017–5019.
10 M. E. Bretado, V. G. Velderrain, D. L. Gutierrez, V. C. Martinez and A. L. Ortiz, *Catal. Today*, 2005, **107–108**, 863–867.
11 M. J. Venegas, E. Fregoso-Israel and H. Pfeiffer, *Ind. Eng. Chem. Res.*, 2007, **46**, 2407–2412.
12 M. Olivares-Marín, T. C. Drage and M. M. Maroto-Valer, *Int. J. Greenhouse Gas Control*, 2010, **4**, 623–629.
13 R. Mosqueda-Rodríguez and H. Pfeiffer, *J. Phys. Chem. A*, 2010, **114**, 4535–4541.
14 M. Seggiani, M. Puccini and S. Vitolo, *Int. J. Greenhouse Gas Control*, 2011, **5**, 741–748.
15 A. Sanna, I. I. S. Ramli and M. Mercedes Maroto-Valer, *Appl. Energy*, 2015, **156**, 197–206.
16 R. Quinn, R. J. Kitzhoffer, J. R. Hufton and T. C. Golden, *Ind. Eng. Chem. Res.*, 2012, **51**, 9320–9327.
17 I. C. Romero-Ibarra, J. Ortiz-Landeros and H. Pfeiffer, *Thermochim. Acta*, 2013, **567**, 118–124.
18 Y. Duan, H. Pfeiffer, B. Li, I. C. Romero-Ibarra, D. C. Sorescu, D. R. Luebke and J. W. Halley, *Phys. Chem. Chem. Phys.*, 2013, **15**, 13538–13558.
19 E. Carella and M. T. Hernandez, *Ceram. Int.*, 2014, **40**, 9499–9508.
20 S. Y. Shan, Q. M. Jia, L. H. Jiang, Q. C. Li, Y. M. Wang and J. H. Peng, *Ceram. Int.*, 2013, **39**, 5437–5441.
21 F. Duran-Muñoz, I. C. Romero-Ibarra and H. Pfeiffer, *J. Mater. Chem. A*, 2013, **1**, 3919–3925.
22 I. C. Romero-Ibarra, F. Durán-Muñoz and H. Pfeiffer, *Green H. Gases*, 2014, **4**(1), 145–154.
23 Z. Zhang, B. Wang, Q. Sun and L. Zheng, *Appl. Energy*, 2014, **123**, 179–184.
24 K. Kanki, H. Maki and M. Mizuhata, *Int. J. Hydrogen Energy*, 2016, **41**(2), 18893–18899.
25 S. M. Amorim, M. D. Domenico, T. L. P. Dantas, H. J. José and R. F. P. M. Moreira, *Chem. Eng. J.*, 2016, **283**, 388–396.
26 P. V. Subha, B. N. Nair, A. Peer Mohamed, G. M. Anilkumar, K. G. K. Warrier, T. Yamaguchi and U. S. Hareesh, *J. Mater. Chem. A*, 2016, **4**, 16928–16935.
27 M. T. Izquierdo, A. Turana, S. García and M. M. Maroto-Valer, *J. Mater. Chem. A*, 2018, **6**, 3249–3257.
28 H. Pfeiffer, P. Bosch and S. Bulbulian, *J. Nucl. Mater.*, 1998, **257**, 309–317.
29 V. L. Mejia-Trejo, E. Fregoso-Israel and H. Pfeiffer, *Chem. Mater.*, 2008, **20**, 7171–7176.
30 Investing New Network, May 2018, https://investingnews.com/daily/resource-investing/energy-investing/lithium-investing/lithium-producing-countries/.
31 H. K. Rusten, E. Ochoa-Fernández, H. Lindborg, D. Chen and H. A. Jakobsen, *Ind. Eng. Chem. Res.*, 2007, **46**, 8729–8737.
32 Z. Qi, H. Daying, L. Yang, Y. Qian and Z. Zibin, *AIChE J.*, 2013, **59**(3), 901–911.
33 H. S. C. Outokumpu, Chemistry For Windows, Version 6.1, Outokumpu Research Oy, Finland, 2009.
34 J. Rodríguez-Carvajal, *Phys. B*, 1993, **192**, 55–69.
35 V. Kaplan, E. Wachter and I. Lubomirsky, *J. Chem. Thermodyn.*, 2011, **43**(11), 1623–1627.
36 M. Sopicka-Lizer, High-Energy ball milling, *Mechanochemical Processing of nanopowders*, Woodhead Publishing, Oxford, 1st edn, 2010.
37 I. A. Carbajal Ramos, J. J. Andrade Gamboa, A. M. Condó and F. C. Gennari, *Solid State Ionics*, 2017, **308**, 46–53.
38 R. B. Khomane, B. K. Sharma, S. Saha and B. D. Kulkarni, *Chem. Eng. Sci.*, 2006, **61**, 3415–3418.